Dispersion in Non-ideal Packed Beds

U. M. Scheven
REQUIMTE/CQFB, Departamento de Química, FCT-Universidade Nova de Lisboa, 2829-516 Caparica, Portugal

DOI 10.1002/aic.11993
Published online August 26, 2009 in Wiley InterScience (www.interscience.wiley.com).

This work reanalyzes published time series dispersion traces (Han et al., AIChE J. *1985;31:277–288) from step input tracer passages recorded at different locations along the length of a packed bed filled with monodisperse solid spheres. The intrinsic dispersivity and sample dependent dispersion are separated by imposing a heuristic model where coarse grained axial advection velocities vary in a plane perpendicular to the flow but not along the direction of flow. The derived intrinsic dispersivity agrees with the predicted value (Scheven et al.,* Phys Rev Lett. *2007;99:054502-1–054502-4). It serves as a bench mark for different implementations of simulations coupling Stokes flow and diffusion in random geometries, and for experimental tests of injection and packing methods. Conceptually, a well defined and fittable effective dispersivity is introduced in an analytical framework describing dispersion data obtained in non-ideal packed beds, where elution profiles cannot be fitted to the solution of the one dimensional advection diffusion equation.* © 2009 American Institute of Chemical Engineers
AIChE J, 56: 289–297, 2010
Keywords: dispersion, packed beds, intrinsic dispersivity, injection and packing effects, tracers

Introduction

Miscible axial tracer dispersion in laminar flow of interstitial mean velocity v through random packs of monodisperse solid spheres with diameter d is of fundamental and long standing interest to chemical engineering research, and it has been studied theoretically[1–5] and experimentally by many groups since the 1950's[6] using tracer experiments; a subset of canonical experimental results[7–12] is reproduced in Figure 1. Since 1996, Nuclear Magnetic Resonance (NMR)[13–26] experiments have also been used to measure D^*_{xx} and volume averaged displacement distributions in flow through packed beds, where the fluid itself — typically water — acts as the tracer. In general, the experimental results exhibit considerable scatter from one report to the next, as indicated by the scatter of Figure 1a. Figure 1b replots the same data on a semi-log plot of normalized dispersivity $l/\lambda = (D^*_{xx}/D_m)/Pe$ vs. Péclet number, with a line representing the universal intrinsic dispersivity $l_d(Pe)/\lambda$ derived from recent NMR measurements of dispersion in measurably different samples of packed monodisperse spheres.[13] The scaling factor $\lambda = d\varepsilon/(1-\varepsilon) = 6r_h$ is chosen by convention[27]; r_h is the hydrodynamic radius of the pack and ε is its porosity. The intrinsic dispersivity is the dispersivity one would get from an infinite medium, with no wall or heterogeneous packing effects. It sets a lower bound on experimentally achievable dispersivities, and is therefore of interest to the researcher wishing to optimize the quality of packings, reactor geometries, or flow injection. The analytical method introduced in this article is used to determine the intrinsic dispersivity of a packed bed from traditional tracer breakthrough data, rather than NMR experiments. It is based on a heuristic model for macroscopic flow heterogeneities where coarse grained axial advection velocities vary in a plane perpendicular to the flow only, and not along the direction of flow. The model is used to calculate the slope of a tracer breakthrough curve, which is related to a well defined but sample dependent axial dispersivity $l_{eff} = l_s + l_d$, where l_d is the universal intrinsic dispersivity of the pack and l_s is a sample dependent and systematic contribution. l_s is calculated to be proportional to the distance between the tracer injection point and the position of the measurement, a prediction corroborated by experiment. Additionally, the intrinsic dispersivity l_d derived from the present analysis extends in a consistent manner the

Correspondence concerning this article should be addressed to U. M. Scheven at ums@dq.fct.unl.pt

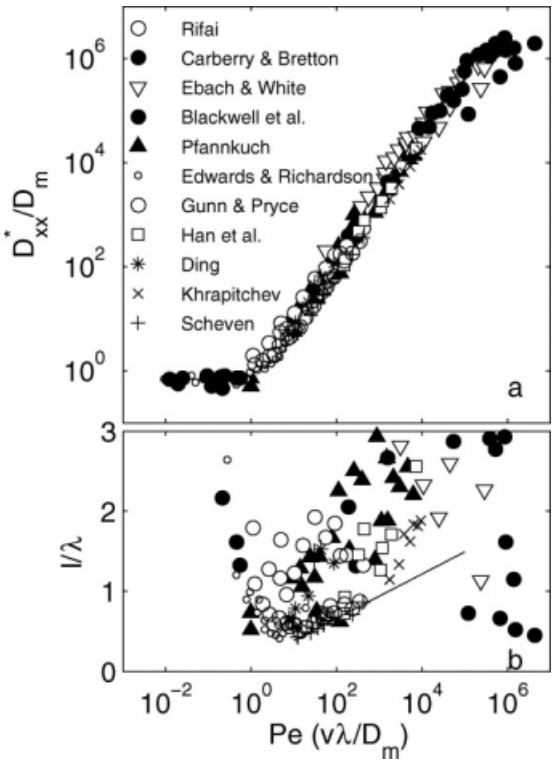

Figure 1. (a) Axial dispersion coefficients D^*_{xx} normalized by molecular diffusion, as a function of Péclet number. (b) Axial dispersivities l normalized by $\lambda = 6r_h$, where λ is the length scale used to define the Péclet number and r_h is the hydrodynamic radius ($Pe = v\lambda/D_m$ and $l/\lambda = (D^*_{xx}/D_m)/Pe$).

NMR-derived results for the universal intrinsic dispersivity of a random pack of spheres.

This article is structured as follows. First, the scanned raw data from the work of Han, Bahkta, and Carbonell[28] (HBC) are presented and the relevant experimental parameters are given. This is followed by a discussion of one-dimensional dispersion and the 1d step input response in a tracer displacement experiment; the 1d model is appropriate for homogeneous flow and, following common practice, was used in the original work to analyze the observed step input responses. This 1d analysis is repeated and followed by a quantification of the long tails and bulk arrivals observed in the break through data. Then the 1d model for homogeneous flow is extended to formulate a new model allowing for small but non-negligible variations of the axial drift velocity over the cross section of the pack. The slope of the tracer breakthrough curve in this model is calculated. HBC's data are then reanalyzed using this extended model, to separate the intrinsic dispersivity of the pack from that caused by macroscopic flow heterogeneities. The intrinsic dispersivity is used to confirm and extend the earlier NMR-based findings. The observed linear growth of effective dispersivity with position and the correct measurement of the universal intrinsic dispersivity validate the model. The conclusion summarizes findings and states their implications for theories and simulations, and proposes a suitable and easily obtainable metric for assessing the quality of packings of spheres and of injectors.

Experiments and 1-d Analysis

HBC investigated longitudinal and lateral dispersion in packed beds, as a function of position in the bed, of Péclet number, and of particle size distribution, measuring the spread of tracers advected through packs contained in a vertical container with square cross section $A = 0.27$ m $\times$ 0.27 m and length $L = 1.5$ m. Five conductivity probes labelled $P_1 \ldots P_5$ were embedded within the walls along the long direction of the container, at $x_1 = 0.028$ m directly behind the inlet at the top and at $x_2 = 0.257$ m, $x_3 = 0.74$ m, $x_4 = 1.121$ m, $x_5 = 1.47$ m along the bed. Monodisperse spheres of diameter $d = 0.0035$ m were filled into the container to produce a packing of mean porosity $\varepsilon = 0.41$, determined from the weight of the pack and the known density of the particles. The interstitial space was then filled with sucrose solution density matched to the NaCl-solution used subsequently as a tracer. At time $t = 0$ a step function input of NaCl-solution (NaCl diffusion coefficient $D_m = 1.545e^{-9}$m^2/s) was injected at the top of the pack with constant volumetric displacement flow. As the conductive NaCl-solution replaced the sucrose solution readings $R(t)$ of the conductivity probes were recorded continuously, starting at $t = 0$. The arrival and passage of the tracer front at each probe location produced a smoothed step rise of conductivity, proportional to the local average tracer concentration. HBC analyzed these data by fitting them to the functional form of uniform displacement flow with constant dispersion coefficients, to obtain dispersion coefficients at positions $x2 \ldots x5$, for four Péclet numbers (940, 1455, 2095, 3445). They presented one set of raw data for the last four conductivity probes, which was scanned form the original publication with a resolution of 600 dots/inch and which is reproduced here in Figure 2. It shows the conductivity parameter $(R - R_{min})/(R_{max} - R_{min})$ which is taken to equal a cross-sectional average of the time dependent tracer concentration c at each probe location x_n. The axial position of each sensor is indicated next to the corresponding curve. These are the time series data analyzed in this article.

The original analysis of the data took the bed to be one a dimensional and semi-infinite medium of dispersion coefficient D_{xx} in which a tracer solution flows with mean velocity v. For $t < 0$, the tracer concentration $c = 0$ everywhere. At $t = 0$, a step input of tracers is made at $x = 0$, with input tracer concentration $c = 1$. The tracer concentration at $x = +\infty$ is zero. The evolution of tracer concentrations is governed by the 1-d advection diffusion equation

$$D_{xx}\frac{\partial^2 c}{\partial x^2} - v\frac{\partial c}{\partial x} = \frac{\partial c}{\partial t} \tag{1}$$

which, for the described initial and boundary conditions is solved by

$$c = \frac{1}{2}\left[\mathrm{erfc}\left(\frac{x - vt}{2\sqrt{D_{xx}t}}\right) + \exp\left(\frac{vx}{D_{xx}}\right)\mathrm{erfc}\left(\frac{x + vt}{2\sqrt{D_{xx}t}}\right)\right] \tag{2}$$

where the first term corresponds to a tracer front of width $\sqrt{D_{xx}t}$ traveling in the positive x direction with velocity v, whereas the second term is negligible for $x \gg \sqrt{D_{xx}t}$, when

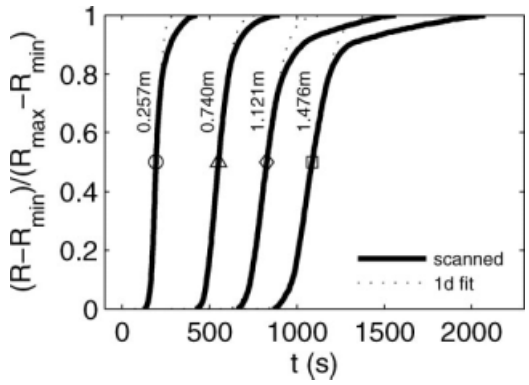

Figure 2. Concentration readings as a function of time measured with four conductivity probes P_2 ... P_5 along the length of the packed bed. A front of conductive NaCl solution displaces density matched sucrose solution, with mean velocity $v_0 = 1.331 \times 10^{-3}$ m/s.

the tracer front is far from the inlet. It is neglected from here on. At the center of the tracer front, defined by $x = vt$ the concentration is

$$c|_{x=vt} = \frac{1}{2} \tag{3}$$

and its time derivative is given by

$$\left.\frac{\partial c}{\partial t}\right|_{x=vt} = \frac{1}{2\sqrt{\pi}}\frac{v}{\sqrt{Dt}} = \frac{1}{2\sqrt{\pi}}\frac{v}{\sqrt{l_d x}} \tag{4}$$

with $D_{xx} = l_d v$, where l_d is the Péclet number dependent dispersivity of the medium. HBC fitted the four time series data sets of Figure 2 to expression 2, leaving the mean flow velocity v and the unknown effective dispersion coefficient D^*_{xx} as free parameters. This fit is repeated here for comparison. Figure 3a plots the fitted values for v, scaled as the Péclet number for convenience. They agree with each other to within a few percent and identify the experiment as the one conducted at $Pe = 2095$. (In the original article, the Péclet number is misidentified with $Pe = 980$.) The low velocity reading at the first sensor indicates less dense packing at the top of column, an effect also observed and remarked upon by HBC. The fitted dispersion coefficients scaled by the molecular diffusivity D^*_{xx}/D_m are shown in 3b with solid circles and errorbars, while the original fitted values for $Pe = 2095$ are indicated by the dashed line. The data were fitted in the concentration range $c \in [0.1, 0.775]$, and error bars indicate the variation of fit results with the choice of fitting domain ranging from $c \in [0.2, 0.675]$ to $c \in [0, 0.875]$. The approximate agreement between new and old fits confirms that the same analysis of the same data produces similar results. However, the significant variation of the fit result with choice of fit range is a direct consequence of the inadequacy of the 1d model being fitted to. This inadequacy is also responsible for the deviation of the fit from the data in the "long tails" at concentrations above $c \approx 0.85$. The 1d model's assumption of a uniform drift velocity — a distribution of drift velocities having zero width — is too restrictive to describe the experiments.

Before proposing and calculating measurable quantities for a less restrictive model of dispersion we quantify the fraction and mean velocity of tracers associated with long tails of the breakthrough curves, and with the bulk arrival of the tracer front. To do so we replot the concentration time series data c vs. t of Figure 2 as concentration versus the normalized deviation of the effective velocity from the mean velocity v_n. At position x_n the normalized deviation is $\beta' = (v_{\text{eff}} - v_n)/v_n$, where $v_{\text{eff}} = x_n/t$ and $v_n = \langle v_{\text{eff}} \rangle$. This is shown in Figure 4. The near coincidence of curves from the probes located at x_3, x_4 and x_5 for concentration $0 < c < 0.85$ indicates that macroscopic and coherent flow heterogeneities affect significantly the dispersion process beyond position x_3, while the curve at x_2 is 'different', presumably due to the higher porosity at the top of the column. Each curve can be used to construct a normalized distribution of effective velocities $P'(\beta') = -(dc/d\beta')$ about the mean velocity v_n; they are shown in Figure 5. They look somewhat similar from one probe to the next. The curves can be approximated reasonably well with a sum of a 'fast' and 'slow' Gaussian distribution to account for the main peak and the long tails in the distribution, respectively. The two Gaussians are plotted individually with dotted lines, while the solid line shows the sum of the two. The fast Gaussian curves are centered at values of $\beta' = b_f \approx 0.025$ indicated by the arrows in Figure 5 and account for roughly 93% of the weight of the distribution for probes P_3, P_4, and P_5; the remainder belongs to the tails. Figure 6 plots three scalar parameters of the four distributions, the mean velocity v_n, the center b_f of the fast Gaussian, and its weight a_f, as a

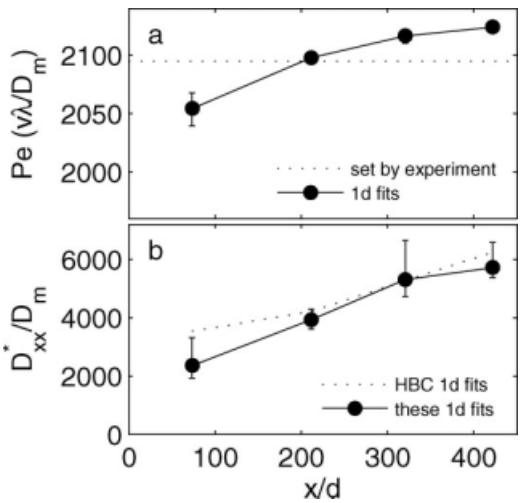

Figure 3. Fits to one dimensional dispersion in the domain $c \in [0.1, 0.775]$ yield effective velocities, plotted as Péclet number in (a); the dashed line indicates the nominal Pe value. (b) Effective dispersion coefficients, normalized by diffusion, as a function of position along the bed. Error bars correspond to changes of the fit range from $c \in [0.2, 0.675]$ to $c \in [0, 0.875]$. Dashes indicate original results.

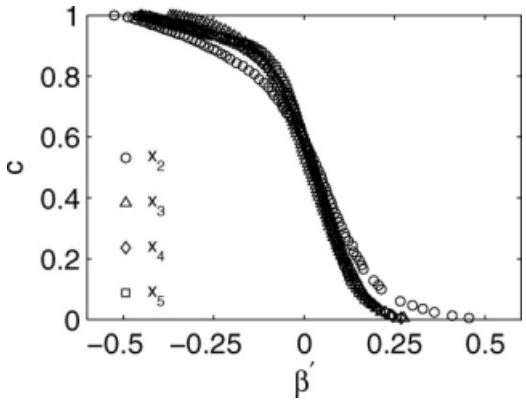

Figure 4. Tracer concentration c vs. normalized deviation of the effective velocity $\beta' = (v_{eff} - v_n)/v_n$, $v_{eff} = x_n/t$, from the mean velocity $v_n = \langle v_{eff} \rangle$. The subscript n identifies the probe number.

function of probe location. The fast Gaussian peaks were fitted over $\beta' \in [-0.15, 0.25]$. Probe P_2 at location x_2 shows entrance effects, with a lower mean velocity attributed to a higher porosity and significantly different location and weight of fast Gaussian distribution, when compared with the respective values at probes P_3, P_4, and P_5.

A Heuristic Model for Small Flow Heterogeneities

The flow field through a pack of solid spheres within a tube may be heterogeneous macroscopically for several reasons, including faster flow near walls,[29] or due to slightly non-uniform flow injection at the ends of the pack, or due to macroscopic variations in the packing density or order, depending on how the sample was made. Some of this macroscopic heterogeneity will now be built into a simple model, in view of the similarity of effective velocity distributions $P'(\beta')$ of Figure 5, and bearing in mind the issue of faster flow near walls. The tube axis and mean flow direction are collinear and taken to be along the x-direction, whereas coordinates y and z specify positions in the cross-section C of the pack perpendicular to the tube axis. Let us define the local mean axial velocity $\overline{v}(x, y, z)$ as the average velocity within a coarse graining length l_c of the pore at (x, y, z), with l_c taken to be on the order of a few sphere diameters. (For a comprehensive discussion of spatial coarse graining, see Ref. 7.) We now assume $\overline{v}$ to be translationally invariant Stokes flow along the x-direction, depending only on position in a plane perpendicular to the tube axis: $\overline{v}(y, z) = v_0(1 + \beta(y, z))$, where $\beta(y, z) \ll 1$. Next, define the β-density $P_v(\beta)$ as the fraction of the cross-sectional area associated with values of β between β and $\beta + d\beta$. The distribution is normalized $\int P_v(\beta)d\beta = 1$ and has zero mean $\int \beta P_v(\beta)d\beta = 0$ because $\langle \overline{v} \rangle = v_0$. Unlike the distribution of effective velocities $P'(\beta')$, the distribution of true advection velocities $P(\beta)$ remains unknown and is not measured directly, though we shall see that its variance can be determined from the data analyzed here. Now, for a translationally invariant velocity distribution a step input of tracers injected at the inlet position (y_i, z_i) will travel through the pack with the approximate velocity $\overline{v}(y_i, z_i) \approx v_0(1 + \beta(y_i, z_i))$ and at time t will have been displaced by $\approx v(y_i, z_i)t$. The expression is approximate only because transverse dispersion of tracers smoothes out some of the lateral velocity variations parameterized by $\beta(y, z)$, over distances set by the transverse coupling length $l' = \sqrt{2l_t x}$, where l_t is the transverse dispersivity, and x is the position along the direction of flow. Fortunately, this transverse dispersivity is small; it can be estimated to be $l_t \approx d/4$ by simple arguments, and measured transverse dispersion coefficients — including the ones reported by HBC — are considerably smaller, yet. The estimated lateral coupling length then ranges from $l'/d \approx 6$ at $x_2 = 0.27$ m to $l'/d \approx 14$ at $x_5 = 1.47$ m. These are of similar order of magnitude, and on the order of the coarse graining length l_c invoked in the construction of $\overline{v}$ and hence $P_v(\beta)$ above; all are much smaller than the width of the bed. Hence, transverse coupling is poor, and translationally invariant velocities $\overline{v}(y, z)$ produce mean tracer displacements equal to $\overline{v}(y, z)t$, indeed. It is, therefore, reasonable to approximate the measurable cross sectional average of the tracer concentration in the bed $c(x, t)$ as an integral over (y, z) of a distribution of 1-d solutions Eq. 2 to the advection diffusion equation, with distributed drift velocities $\overline{v}(y, z) = v_0(1 + \beta(y, z))$.

$$c = \frac{1}{2}C^{-1} \iint \mathrm{erfc}(g(\beta(y, z)))dydz$$

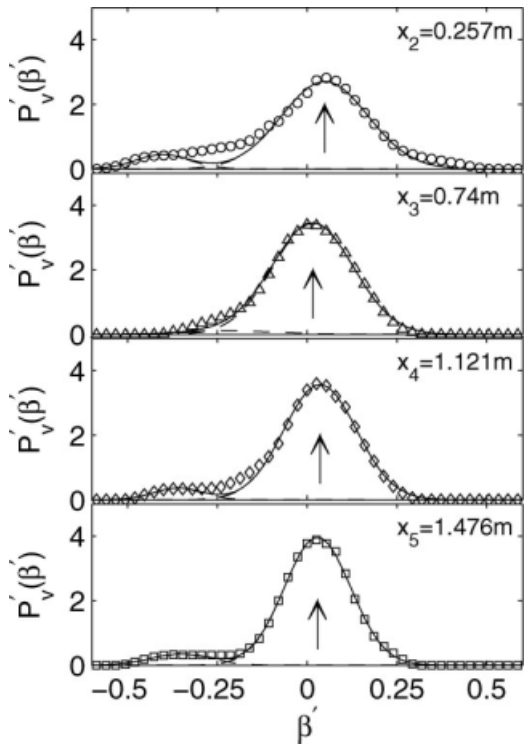

Figure 5. Distributions of effective velocities $P'(\beta') = -dc/d\beta'$, where $\beta' = (v_{eff} - v_n)/v_n$, with $v_{eff} = x_n/t$ and $v_n = \langle v_{eff} \rangle$. The distributions are approximated by the sum (solid line) of a fast gaussian distribution of weight a_f, centered at $\beta' = b_f$ and a small and slower gaussian distribution accounting for the observed tails in the data.

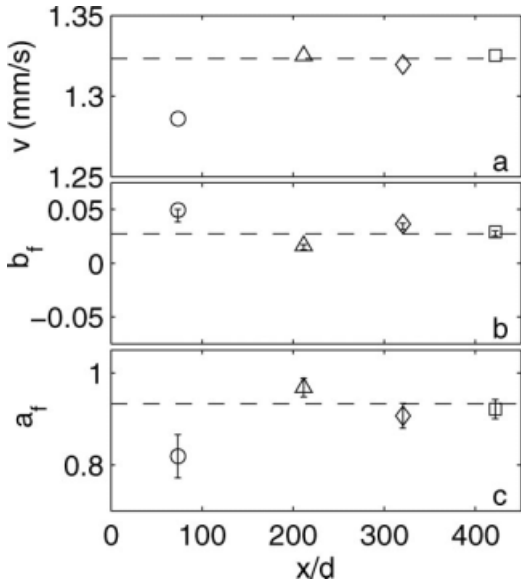

Figure 6. Plots against probe location of (a) mean flow velocity $v_n = x_n/t_n$, (b) center b_f of the fast gaussian component of the $P'(\beta')$, (c.f. arrows of Figure 5), and (c) weight a_f of the fast gaussian component, obtained in the fitting domain $\beta' \in [-0.15, 0.25]$.

The dashed lines indicate the averages over probes P_3, P_4, P_5 for which the distributions of effective velocities are similar.

where C is the cross-sectional area, and the errorfunction in the integrand describes the traveling tracer front of expression 2 and the argument of the error function is given by expression 6 below. Because the integrand depends on y and z only through $\beta(y, z)$ this can be rewritten as an integral in β,

$$c = \frac{1}{2}\int P_v(\beta)\mathrm{erfc}(g(\beta))d\beta \tag{5}$$

$$g = \left(\frac{x_n - v_n(1+\beta)t}{2\sqrt{l_d v_n(1+\beta)t}}\right) \tag{6}$$

where we have also rewritten the dispersion coefficient $D_{xx} = l_d \times v_n\ (1 + \beta)$ in terms of the intrinsic dispersivity l_d, the mean flow velocity v_n at location x_n, and β. We differentiate Eq. 5 and exchange the order of integration and differentiation to obtain

$$\left(\frac{\partial c}{\partial t}\right) = -\frac{1}{\sqrt{\pi}}\int P_v(\beta)\left(\frac{\partial g}{\partial t}\right)e^{-g^2}d\beta \tag{7}$$

with

$$\left(\frac{\partial g}{\partial t}\right) = -\frac{v_n(1+\beta)}{4\sqrt{l_d}}\frac{(x_n + v_n t(1+\beta))}{(v_n t(1+\beta))^{\frac{3}{2}}}. \tag{8}$$

The rate of change of the tracer concentration can be determined experimentally at four different probe locations x_n, at times t_m when the tracer front passes the respective probe. It is convenient to parameterize the time of measurement t_m in terms of a small scalar parameter δ, such that $t_m = x_n/v_n(1 + \delta)$. For $\delta = 0$, the measurement occurs within the steep rise of the tracer concentration, at each location x_n. Expression 8, rewritten in terms of the parameter δ, becomes

$$\left(\frac{\partial g}{\partial t}\right) = -\frac{v_n}{2\sqrt{x_n l_d}}\sqrt{\frac{1+\delta}{1+\beta}}\left(1 + \frac{\delta}{2} + \frac{\beta}{2}\right) \tag{9}$$

The exponential e^{-g^2} in the integrand of Eq. 7 can be rewritten as

$$e^{-g^2} = \exp\left(-\frac{x_n}{4l_d}\frac{(\delta-\beta)^2}{(1+\delta)}\right)\times \exp\left(\frac{x_n}{4l_d}\frac{\beta(\delta-\beta)^2}{(1+\delta)(1+\beta)}\right). \tag{10}$$

which is a Gaussian in β centered around the parameter δ multiplied by a β-dependent correction factor roughly equal to 1 for $|\beta| \lesssim 0.3$, $|\delta| \lesssim 0.1$. Note that the correction factor is exactly equal to 1 for $\beta = \delta$, the only values of β and δ where the Gaussian is not negligible, in the limit $x_n/2l_d \gg 1$; this limit applies since $l_d \approx \mathcal{O}(d)$ and d was the diameter of a particle. Combining terms from Eqs. 9 and 10 to define

$$A(\beta,\delta) = \sqrt{\frac{1+\delta}{1+\beta}}\left(1 + \frac{\delta}{2} + \frac{\beta}{2}\right)\times \exp\left(\frac{x_n}{4l_d}\frac{\beta(\delta-\beta)^2}{(1+\delta)(1+\beta)}\right) \tag{11}$$

the time derivative of the tracer concentration Eq. 7, evaluated at time of measurement $t_m = x_n/v(1 + \delta)$, becomes

$$\left(\frac{\partial c}{\partial t}\right) = \frac{v_n}{2\sqrt{\pi x_n l_d}}\int P_v(\beta)A(\beta,\delta)\exp\left(-\frac{x_n}{4l_d}\frac{(\delta-\beta)^2}{(1+\delta)}\right)d\beta \tag{12}$$

Now we shall consider the effect of 'on time' arrivals with that produced by 'late' arrivals — the observed long tails — on the measurement at $t_m = x_n/v(1 + \delta)$. Let us assume for convenience that a component P_c of the unknown distribution of velocities $P(\beta)$ is Gaussian, with amplitude a, center b and variance σ_c^2.

$$P_c = \frac{a}{\sqrt{2\pi}\sigma_c}\times\exp\left(-\frac{(b-\beta)^2}{2\sigma_c^2}\right) \tag{13}$$

Tracers belonging to this component of the velocity distribution arrive, on average, at position x_n at time $t_a = x_n/v_n(1 + b)$, but the slope $(\partial c/\partial t)$ is measured at time $t_m = x_n/v_n(1 + \delta)$. Inserting Eq. 13 into Eq. 12 and completing the squares in the exponents leads to

$$\left(\frac{\partial c}{\partial t}\right) = \frac{a v_n G_s(b,\delta)}{2\sqrt{\pi x_n l_d}}\int A(\beta,\delta)e^{-(f(\beta)-f_0)^2}d\beta \tag{14}$$

with

$$G_s(b,\delta) = \exp\left(-\frac{(\delta-b)^2}{(2\sigma_c^2 + 4(1+\delta)l_d/x_n)}\right)$$

$$f(\beta) = \beta\sqrt{\frac{x_n}{4l_d}\frac{1}{(1+\delta)} + \frac{1}{2\sigma_c^2}}$$

$$f_0 = \left(\frac{x_n}{4l_d}\frac{\delta}{(1+\delta)} + \frac{b}{2\sigma_c^2}\right) \Bigg/ \sqrt{\frac{x_n}{4l_d}\frac{1}{(1+\delta)} + \frac{1}{2\sigma_c^2}}$$

The Gaussian prefactor $G_s(b, \delta)$ clearly suppresses the contribution of components $P_c(\beta)$ corresponding to 'early and late arrivals', with respect to the time of measurement, where $(\delta - b)^2$ is not small. On the other hand, $G_s(b, \delta) = 1$ if one chooses to evaluate the slope of the tracer curve at the arrival time associated with $P_c(\beta)$, by setting $\delta = b$. For the approximately bi-modal distributions of Figure 5 the value of $(\partial c/\partial t)$ measured at the arrival time of the large Gaussian peak $\delta = b_f \approx 0.025$ is therefore dominated by that peak; the contribution of the late arrivals to measured $(\partial c/\partial t)$ is comparatively smaller by a factor $G_s(a_s/a_f) \lesssim 0.01$ and thus negligible.

We therefore choose the measurement time by setting $\delta = b_f$ for each breakthrough curve, which corresponds to measuring the slope of the breakthrough curve where the slope is maximal. Expression (14) can then be integrated, after replacing $A(\beta, \delta)$ of expression 11 with its Taylor series expansion in β, about $\beta_0 = \delta$. This leads to

$$\left(\frac{\partial c}{\partial t}\right) = \frac{a v_n}{2\sqrt{\pi l_d x_n}}\frac{1}{\sqrt{1+\sigma_c^2 x_n/2l_d}} \times \left[1+\delta+\left(\delta+\frac{2l_d}{x_n}\right)\left(\frac{\sigma_c^2 x_n}{\sigma_c^2 x_n + 2l_d(1+\delta)}\right)\right]. \quad (15)$$

The odd powers of the Taylor series in $(\beta - \delta)^n$ integrate to zero by symmetry, while the 0th and 2nd order terms are linear in the small paramaters δ and $4l_d/x_n$; higher order terms involve higher powers in these small parameters and can be dropped. As a check, result Eq. 15 reduces to expression 4 for the case of homogeneous flow, where $a = 1$, $\sigma_c^2 = 0$ and $\delta = 0$. Squaring Eq. 15 and rearranging terms one obtains an expression for a measurable "effective" dispersivity.

$$l_{\text{eff}} = \frac{v_n^2}{4\pi(\partial c/\partial t)^2 x_n} = \frac{1}{a^2}\left(l_d + \frac{1}{2}\sigma_c^2 x_n\right)\left[1+\delta+\left(\delta+\frac{2l_d}{x_n}\right) \times \left(\frac{\sigma_c^2 x_n}{\sigma_c^2 x_n + 2l_d(1+\delta)}\right)\right]^{-2} \quad (16)$$

To assess the validity of this expression, recall that it was obtained assuming the dominant Gaussian peak in effective velocities to be caused by a convolution of two processes giving rise to Gaussian spreading, stochastic diffusion coupled to mechanical mixing on the one hand, with spatial variance $2l_d x_n$, and the deterministic spread of tracers on the other hand, where the assumed assumed Gaussian velocity distribution Eq. 13 with variance σ_c^2 spreads tracers with variance $\sigma_c^2 x_n^2$. The use of a Gaussian velocity distribution to approximate the true $P(\beta)$ is a reasonable way of introducing a $P(\beta)$ with finite width as long as $\sigma_c^2 x_n^2 \lesssim 2l_d x_n$, and $P(\beta)$ is reasonably compact. In this limit

$$l_{\text{eff}} \times a^2(1+\delta)^2 = l_d + \frac{1}{2}\sigma_c^2 x_n \quad (17)$$

where the left hand side contains measurable quantities, and the right hand side is the sum of a universal quantity, l_d, and a linear term in x which depends on the quality of flow injection, wall effects, and perhaps other particulars of the experiment.

In the next section, tracer concentration data is analyzed using expressions 16 and 17. There are two parameters to be fitted, the unknown variance σ_c^2 of the distribution of drift velocities and the intrinsic dispersivity l_d. The slope $(\partial c/\partial t)$ is determined with polynomial fits to obtain l_{eff}, and the remaining parameters $\delta = b_f$ and $a = a_f$ will be taken from the $P'(\beta')$-derived parameters of Figure 6.

Data Analysis

The first task at hand is to determine $(\partial c/\partial t)$ as the tracer front successively passes the four sensors $P_2 \ldots P_5$. Figure 7 shows the measured time dependent tracer concentration in the range $0.0 < c < 0.9$, referenced to the time $t_n/(1+\delta)$, where $t_n = x_n/v_n$, $v_n = \langle x_n/t \rangle$ as before. The time of measurement is set using $\delta = b_f$, which means that the slope of the breakthrough curve is measured where it is maximal, corresponding to the peaks marked by arrows in Figure 6. The concentration data vary smoothly, exhibiting small systematic scatter introduced by the digitization process. They were fitted to 5th order polynomials in $t - t_n/(1+\delta)$, with fitting domains defined by concentration intervals between $c \in [0.1, 0.6]$ and $c \in [0.1, 0.925]$; the fit in fitting domain $c \in [0.1,$

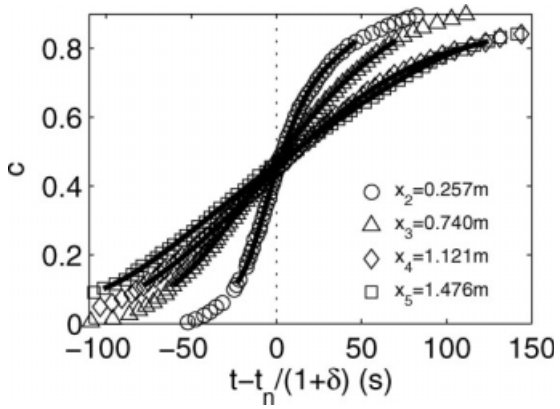

Figure 7. Rise of tracer concentration associated with the passage of one tracer front recorded at the four sensor locations $x_2 \ldots x_5$, plotted as a function of $t - t_n$, with $t_n = x_n/v_0\ (1+\delta)$.

5th-order polynomials ((solid lines)) are fitted to the data to determine the slope $(\partial c/\partial t)$ at $t - t_n = 0$.

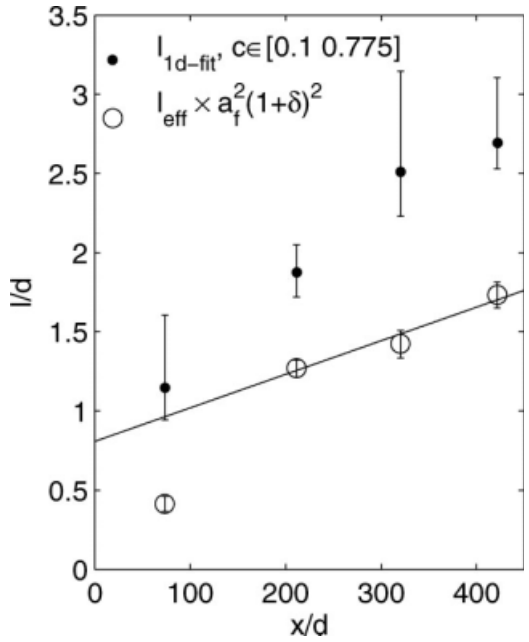

Figure 8. Effective dispersivity scaled by the sphere diameter, as a function of measurement position. For the last three probes P_3, P_4, P_5 the scaled effective dispersivities (open circles) $l_{eff} \times a^2(1 + \delta)^2$ fall onto a straight line.

The error bars on the $a^2(1 + \delta)^2 l_{eff}$ are true error bars representing statistical uncertainty. The error bars on the 1d fit indicate the fit range dependence of the fit result.

0.775] is shown. Unsurprisingly, the polynomial fits are excellent, with a root mean squared deviation of the fits from the data of less than 0.005 concentration units. This compares favorably with the poor 1d fits of the traditional analysis, for which the rms-deviation is four times larger in the same domain. The desired $(\partial c/\partial t)$ are equal to the derivatives of the fitted polynomials evaluated at $t - t_n/(1 + \delta) = 0$. The fitted derivatives and their errors (less than 0.5%) were then used to calculate the effective dispersivities l_{eff} defined in expression 16, along with associated errors. Expression 17 leads us to expect $l_{eff} \times a^2 (1 + \delta)^2$ to lie on a straight line with y-axis intercept $l_d \times (1 + \mathcal{O}(\delta))$ and slope $\approx \sigma_c^2/2$. They do, in Figure 8, where $l_{eff} \times a^2(1 + \delta)^2$ are shown in the figure with large open circles, using the values of a_f and $\delta = b_f$ from Figure 6, with propagated errors. The data for the last three sensors define a straight line whose slope sets $\sigma_c^2 \approx 0.005$, with y-axis intersection near 0.80. Nonlinear least squares fitting to Eq. 16 yields an intrinsic dispersivity of $l_d/d = 0.76 \pm 0.14$. Results from the fit range dependent 1d analysis of Figure 3 are also shown for comparison.

The dependence of final results on the choice of fitting domain was tested by fitting the 5th-order polynomial repeatedly over many fit ranges and carrying out the analysis for each choice of fitting domain. This domain was bounded by a lower concentration limit of 0.1, chosen to omit the initial high curvature of the conductivity readings, and variable upper limit $c_{max} \in [0.6, 0.925]$, where the upper bound restricts the fit range to omit tracer concentrations associated with long tails in the tracer data. l_{eff} and l_d, scaled by the hydrodynamic length $\lambda = d\varepsilon/(1-\varepsilon)$, are plotted in Figure 9 as a function of fitting range for the polynomial fits. The variation with fitting range is negligible and the fits are good for all fitranges that were tested, confirming that the effective dispersivity of Eq. 16 is measurable in a robust manner, with well defined errors. The nonlinear least squares fits of l_{eff} used to calculate l_d are best for the polynomial fit range $c_{max} \in [0.1, 0.775]$, and the systematic variation of fitted l_d/λ with fit range is very small throughout and always less than the statistical error indicated by the error bars. The variation of fitted σ_c^2 is on the order of 10% of the stated value. The value of $l_d/\lambda = 1.1 \pm 0.2$ at $Pe = 2095$ is plotted with a solid circle in Figure 10, in the context of the prior NMR measurements. The straight line in Figure 1b based on these NMR results is thus confirmed and extended, quantitatively and using a traditional tracer experiment. With inclusion of the present result the functional dependence of $l_d/\lambda = A \ln(Pe) + B$ gives $A = 0.131 \pm 0.007$ and $B = 0.07 \pm 0.03$ between $Pe \in [10, 2100]$, where the data point at $Pe = 240$ has been omitted from the fit after systematic evaluation of fit quality flagged it as systematic "outlier".

The intrinsic dispersivity l_d of the packed bed has thus been determined from slope of the breakthrough curves $(\partial c/\partial t)$, and values of (a_f, b_f) determined from the distributions of effective velocities $P'(\beta')$, which in turn were also derived simply from the breakthrough curves. The quality of the pack or the flow injectors was quantified, in terms of the fitted σ_c^2.

Conclusions and Final Remarks

There is satisfactory quantitative agreement of intrinsic dispersivities obtained with different techniques, NMR and

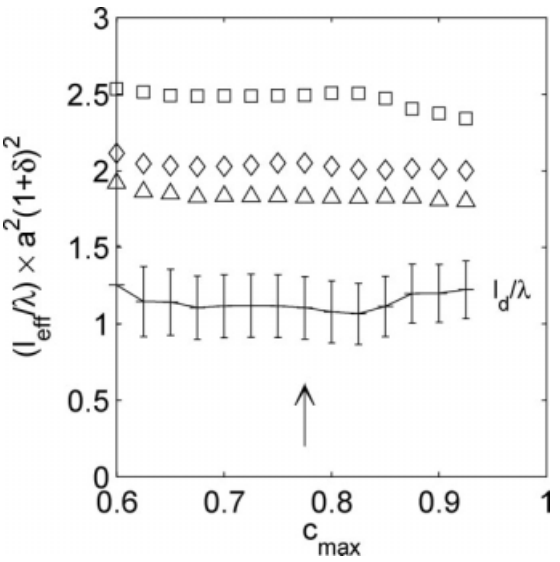

Figure 9. (a) Slope derived scaled effective dispersivities at probe locations x_3, x_4, x_5 and the fitted intrinsic dispersivity l_d/λ, as a function of the largest concentration in the fitting domain for the 5th order polynomial fit of Figure 7.

$\lambda = 6r_h$, r_h is the hydrodynamic radius.

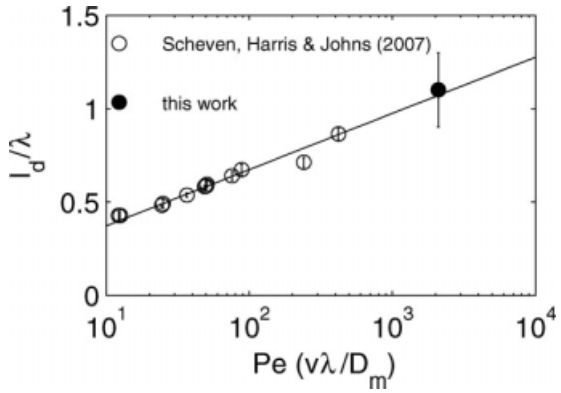

Figure 10. Intrinsic dispersivity scaled by the hydrodynamic length λ, as a function of Péclet number.

From Ref. 13, and this work.

traditional tracer method analyzed here. The experimentally determined scaled intrinsic dispersivity $l_d(Pe)/\lambda$ is a useful universal property of packed beds of monodisperse solid spheres which serves as a benchmark for the validation of computer code simulating creeping flows with diffusion in complex geometries. Simulations in synthetic infinite packs of identical spheres implemented with periodic boundary conditions should reproduce the present results to within the stated errors, as the scaled dispersion results by Maier et al.[30] were shown to do in the NMR work.

$l_d(Pe)/\lambda$ also serves to test two canonical but mutually exclusive theories of dispersion predicting a logarithmic Pe-dependence of dispersivity, Saffman's[1,2] network of randomly oriented identical capillaries with length l and radius a, which has one free parameter, the ratio l/a, and Koch and Brady's model of a dilute pack of spheres,[3] which has no free parameters. The data fit Saffman's model and analysis,[2] for $l/a \approx 4$, as was already seen in the NMR work.[13]

The heuristic working assumption of a translationally invariant velocity distribution along the direction of flow is quantitatively consistent with experimental observations and represents a marked improvement over the assumption of uniform flow in the analysis, at the cost of introducing one free but meaningful parameter, the variance σ_c^2. A conceptually related heuristic assumption about the flow field was also successful in explaining the broad features of non-Gaussian tracer elution curves measured in packs of micro-porous beads.[26] One may surmise that approximate translational invariance of the flow field along the direction of flow be a general feature of flow in packed beds; here it appears to hold for the bottom 75% of the pack probed by P_3, P_4, and P_5, as indicated by the linear growth of effective dispersivities and the correct value of the intrinsic dispersivity.

The slope of l_{eff} vs. position sets the variance $\sigma_c^2 \simeq 0.005$ of the underlying distribution of drift velocities. The rms width $\sigma_c \simeq 7\%$ is of the same order as the variances found by NMR[2] and in simulations of Stokes flow through a packed bed confined to a cylinder[31] of diamater $D = 48d$, where the effective dispersion grows roughly linearly with distance in figure 17 of Ref. 31. The growth rate observed in their simulation result corresponds to $\sigma_c \approx 7.5\%$. If translational invariance were found to hold in general, as one might expect if variations of velocities were indeed dominated by wall effects,[29,31] then it would be worthwhile to establish experimentally the minimum attainable variance σ_c^2 of the underlying distribution of drift velocities, as a function of tube length or packing parameters, as was the original motivation by HBC, or as a function of injector designs. To this end, it would be interesting to reanalyze HBC's or other worker's data, if the raw data became available.

Estimates of attainable σ_c^2 in packs of monodisperse spheres can be derived from other published standard elution experiments, even where the time dependent concentration is measured at the end of the bed alone, rather than at several locations along the tube. It is given by $\sigma_c^2 = \frac{2}{L}(l_{eff} - l_d(Pe))$, where the intrinsic $l_d(Pe)$ is calculated from the universal logarithmic Pe-dependence of the scaled dispersivity l_d/λ with $\lambda = d\varepsilon/(1-\varepsilon)$, the effective dispersivity l_{eff} determined from maximal measured slope of the tracer breakthrough curve, and where L is the length of the tube.

Finally, it is worth remembering that the deviations between the straightforward 1d fit and the breakthrough curves served to indicate the presence of a distribution $P_v(\beta)$ having small but finite width σ_c. An absence of measurable deviations of the data from a 1-d fit the does not imply $\sigma_c = 0$, only that it is small ($\sigma_c^2 L^2 \ll l_d L$). In this case, the distribution of effective velocities will appear to be Gaussian to a very good approximation, whence $a_f = 1$ and $\delta = b_f = 0$. Then Eq. 17 simplifies to

$$l_{eff} = l_d + \frac{1}{2}\sigma_c^2 L. \tag{18}$$

where L is the length of the tube or the axial position where the breakthrough curve is measured. This might also be relevant for beds packed with porous beads, with a redefined intrinsic dispersivity for porous beads depending on additional parameters including bead porosity and the possibly restricted diffusion coefficient within a spherical particle.

Acknowledgments

The author gratefully acknowledges grant PTDC/ENR/65170/2006, by the Fundação para a Ciência e Tecnologia - Ministério de Ciência, Tecnologia e Ensino Superior, Portugal.

Literature Cited

1. Saffman PG. A theory of dispersion in a porous medium. *J Fluid Mech.* 1959;6:321–349.
2. Saffman PG. Dispersion due to molecular diffusion and macroscopic mixing in flow through a network of capillaries. *J Fluid Mech.* 1960;7:194–208.
3. Koch D, Brady JF. Dispersion in fixed beds. *J Fluid Mech.* 1985;154:399–427.
4. Mauri R. Heat and mass-transport in random velocity-fields with application to dispersion in porous-media. *J Eng Math.* 1995;29:77–89.
5. Whitaker S. *The Method of Volume Averaging*. New York: Springer Verlag, 1999.
6. Delgado JMPQ. A critical review of dispersion in packed beds. *Heat Mass Transfer*. 2006;42:279–310, DOI 10.1007/s00231–005-0019–0.
7. Rifai MNE, Kaufman WJ, Todd DK. *Dispersion Phenomena in Laminar Flow Through Porous Media*. Sanitary Engineering Research Laboratory Report. No. 2, IER Series. Berkeley, CA: University of California, 1956:93.

8. Carberry JJ, Bretton RH. Axial dispersion of mass in flow through fixed beds. *AIChE J*. 1958;4:367–375.
9. Ebach EA, White RR. Mixing of fluids flowing through beds of packed solids. *AIChE J*. 1958;4:161–169.
10. Pfannkuch HO. Contribution a létude des déplacements des fluides dans un milieu poreux. *Rev Inst Fr Petrol*. 1963;18:215-ff.
11. Edwards MF, Richardson JF. Gas dispersion in packed beds. *Chem Engr Sci*. 1968;23:109-ff.
12. Gunn DJ, Pryce C. Dispersion in packed beds. *Trans Inst Chem Eng*. 1969;47:T341–T350.
13. Scheven UM, Harris R, Johns ML. Intrinsic dispersivity of randomly packed monodisperse spheres. *Phys Rev Lett*. 2007;99:054502-1–054502-4.
14. Ding A, Candela D. Probing nonlocal tracer dispersion in flows through random porous media. *Phys Rev E*. 1996;54:656–660.
15. Lebon L, Oger L, Leblond J, Hulin JP, Martys NS, Schwartz LM. Pulsed gradient NMR measurements and numerical simulation of flow velocity distribution in sphere packings. *Phys Fluids*. 1996;8:293–301.
16. Tallarek U, Albert K, Bayer E, Guiochon G. Measurement of transverse and axial apparent dispersion coefficients in packed beds. *AIChE J*. 1996;42:3041–3054.
17. Seymour JD, Callaghan PT. Generalized approach to NMR analysis of flow and dispersion in porous media. *AIChE J*. 1997;43:2096–2111.
18. Tallarek U, Dusschooten Dv, As Hv, Bayer E, Guichon G. Study of transport phenomena in chromatographic columns by pulsed field gradient NMR. *J Phys Chem B*. 1998;102:3486–3497.
19. Manz B, Alexander P, Gladden LF. Correlations between dispersion and structure in porous media probed by nuclear magnetic resonance. *Phys Fluids*. 1999;11:259–267.
20. Kandhai D, Hlushkou D, Hoekstra AG, Sloot PMA, Van As H, Tallarek U. Influence of stagnant zones on transient and asymptotic dispersion in macroscopically homogeneous porous media. *Phys Rev Lett*. 2002;88:234501-1–234501-4.
21. Scheven UM, Sen PN. Spatial and temporal coarse graining for dispersion in randomly packed spheres. *Phys Rev Lett*. 2002;89:254501-1–254501-4.
22. Stapf S. NMR investigations of correlations between longitudinal and transverse displacements in flow through random structured media. *Chem Phys*. 2002;284:369–388.
23. Khrapitchev AA, Callaghan PT. Reversible and irreversible dispersion in a porous medium. *Phys Fluids*. 2003;15:2649–2660.
24. Scheven UM, Seland JG, Cory DG. NMR propagator measurements on flow through a random pack of porous glass beads and how they are affected by dispersion, relaxation, and internal field inhomogeneities. *Phys Rev E*. 2004;69:021201-1–021201-9.
25. Scheven UM, Verganelakis D, Harris R, Johns ML, Gladden LF. Quantitative nuclear magnetic resonance measurements of preasymptotic dispersion in flow through porous media. *Phys Fluids*. 2005;17:117107-1–117107-7.
26. Holland DJ, Scheven UM, Middelberg APJ, Gladden LF. Quantifying transport within a porous medium over a hierarchy of length scales. *Phys Fluids*. 2006;18:033102-1–12.
27. Whitaker S. Forced convection heat transfer correlations for flow in pipes, past flat plates, single cylinders, single spheres, and for flow in packed beds and tube bundles. *AIChE J*. 1972;18:361–371.
28. Han NW, Bhakta J, Carbonell RG. Longitudinal and lateral dispersion in packed beds: effect of column length and particle size distribution. *AIChE J*. 1985;31:277–288.
29. Vortmeyer D, Schuster J. Evaluation of steady flow profiles in rectangular and circular packed-beds by a variational method. *Chem Eng Sci*. 1983;38:1691–1699.
30. Maier RS, Kroll DM, Bernard RS, Howington SE, Peters JF, Davis TD. Pore-scale simulation of dispersion. *Phys Fluids*. 2000;12:2065–2079.
31. Maier RS, Kroll DM, Bernard RS, Howington SE, Peters JF, Davis TD. Hydrodynamic dispersion in confined packed beds. *Phys Fluids*. 2003;15:3795–3815.

Manuscript received Dec. 19, 2008, revision received Apr. 28, 2009, and final revision received June 5, 2009.